ROYAL AERONAUTICAL SOCIETY

REGULAR PAPER

A parametric design approach for multi-lobed hybrid airships

M. Manikandan[1], R. R. Shah[2], P. Priyan[1], B. Singh[1,3] and R. S. Pant[2]

[1]Department of Aeronautical and Automobile Engineering, Manipal Institute of Technology, Manipal Academy of Higher Education, Manipal, 576104, Karnataka, India, [2]Department of Aerospace Engineering, Indian Institute of Technology Bombay, Mumbai, 400076, Maharashtra, India and [3]Department of Aerospace Engineering, Faculty of Engineering, Universiti Putra Malaysia, Serdang, 43400, Selangor, Darul Ehsan, Malaysia
Corresponding author: B. Singh; Email: balbir.s@manipal.edu

Abstract

In recent years, there has been an increasing interest in the research and development of hybrid airships for various applications. Airship design involves multiple design parameters from various disciplines that interact mutually. Existing design methodologies, however, are often limited to fixed shapes and geometry. This paper provides a comprehensive parametric design approach for the sizing of multi-lobed hybrid air vehicles for low- and high-altitude applications. The proposed design techniques are robust so that the designer has the freedom to change the number of lobes, the relative location of lobes, the envelope profile, and the optimiser for the design optimisation process. The outcomes of the proposed methodology are envelope volume, wetted surface area, length and span of the envelope, sizing and layout of the solar array, and sizing and layout of the fins. The modeling techniques highlighted in this paper are very efficient for the design and optimisation of multi-lobed airships in the conceptual design phase with a large design exploration space. The robustness of the shape generation algorithms is tested on some of the standard envelope profiles of airships. The effect of the shape and geometry of the multi-lobed envelope on added mass is demonstrated through the added mass estimation using Boundary Element Method.

Nomenclature

A_i	CST shape coefficients
a_i	Gertler shape coefficients
a	Semi-major axis of the central lobe [m]
AR_T	Tail aspect ratio
b	Semi-minor axis of the central lobe [m]
b_T	Tail span [m]
c	Semi-major axis of the outer lobe(s) [m]
C_p	Prismatic coefficient
C_f	Friction coefficient
C_{D0}	Zero-lift drag coefficient
C_{HT}	Horizontal tail volume coefficient
C_{VT}	Vertical tail volume coefficient
C_L/C_D	Aerodynamic efficiency
c.g.	Centre of gravity [m/s^2]
c.b.	Centre of buoyancy from nose [m]
$C_{L\alpha,tail}$	Tail lift curve slope [$per\ deg$]
d	Semi-minor axis of the outer lobe(s) [m]
e	Distance between the centre of the lobes (longitudinal) [m]
f	Distance between the centre of the lobes (lateral) [m]

g	Distance between the centre of the lobes (vertical) [*m*]
ht	Height of the envelope [*m*]
L	Length of the airship [*m*]
l/d	Fineness ratio
L/D	Lift to drag ratio
l_{HT}	Distance between the c.g. and the quarter chord of the horizontal tail [*m*]
l_{VT}	Distance between the c.g. and the quarter chord of the vertical tail [*m*]
l_T	Tail moment arm [*m*]
m	Point of maximum diameter
MAC	Mean aerodynamic chord [*m*]
M	Mach number
N_{lobes}	Number of lobes
N_{fins}	Number of fins
$P_{ellipse}$	Ellipse perimeter [*m*]
P_{lobes}	Lobes perimeter [*m*]
R_0	Nose radius [*m*]
R_1	Tail radius [*m*]
Re	Reynolds number
S_{env}	Envelope surface area [m^2]
S_{wetted}	Wetted surface area [m^2]
S_{HT}	Horizontal tail planform area [m^2]
S_{VT}	Vertical tail planform area [m^2]
S_T	Exposed tail area [m^2]
$S_{T,total}$	Total tail area [m^2]
$TOGW$	Take-off gross weight [kg]
V_{env}	Envelope volume [m^3]
W	Width of the airship [*m*]
X_s	Starting point of the solar array [*m*]
X_f	Ending point of the solar array [*m*]
ψ	Non-dimensional spatial coordinate (x-direction)
ζ	Non-dimensional spatial coordinate (y-direction)
θ_{array}	Intended angle of array [deg]
Δ	Tail sweep angle [deg]
Γ	Tail dihedral angle [deg]

1. Introduction and background

Designing an airship is a very challenging task in terms of parameterising the geometry with a minimum number of variables to incorporate the effect of various disciplines on its sizing and performance. In recent years, design studies on airships have seen significant development because of their potential for various civil and defense applications. There is a huge demand in the market for lighter-than-air (LTA) systems for heavy cargo transportation and long-endurance high-altitude applications.

Among the types of LTA systems, hybrid airships with multiple lobes have become attractive and ideal platforms for various applications in recent years. A multi-lobed hybrid airship is a type of airship that combines the features of both traditional blimps and rigid airships. It is characterised by its unique shape, which consists of multiple lobes or cells that are interconnected, allowing for greater stability and manoeuverability. These hybrid airships use a combination of buoyant gas, such as helium, to provide lift and a system of internal and external support structures to maintain their shape and rigidity. They also often feature propulsion systems, such as engines or propellers, to enable controlled movement through the air. One of the key benefits of multi-lobed hybrid airships is their ability to carry heavy loads over long distances while using significantly less fuel than traditional aircraft. This makes them a potentially attractive option for applications such as cargo transportation and remote area access. However, multi-lobed hybrid airships are still a relatively new technology and there are still challenges to be addressed,

such as the need for specialised infrastructure for takeoff and landing, as well as the potential risks associated with operating large, buoyant structures in close proximity to populated areas.

There are several studies have focused on the conceptual design and optimisation of airships with multi-lobed envelope geometry. The most common observation in the available literature is that a fixed shape and geometry of the envelope is considered. Boyd [1] developed a set of equations that govern the performance of hybrid airships to understand their economic viability. Donaldson et al. [2] introduced a process that can be used for the parametric design of low-emission multi-lobed hybrid air vehicles for cargo transportation. Agte et al. [3] summarised a work performed in the conceptual design of hybrid airship for intra-regional flexible access transport and also presented a derivation of master constraint equation. It focuses on the design and technical aspects of the hybrid lift vehicles and also touches upon on the overall system architecture to identify the key issues involved in the design of hybrid airships. Carichner and Nicolai [4] demonstrated the superiority of hybrid airships over conventional airships in terms of performance through a detailed case study. They presented a comprehensive design methodology to achieve the final configuration of the multi-lobed airship with a fixed envelope shape for given mission requirements. Verma et al. [5] proposed a novel approach to obtain the optimal configuration of the multi-lobed airship in terms of total lift apportionment for different flight-time constraints and altitudes. Ceruti and Marzocca [6] presented a design methodology using the concept of volume fractions to be used in the evaluation of weight, dimensions, and performance in the initial design phase. Mahzan et al. [7] proposed a design methodology for hybrid airships through the investigation of aerodynamic characteristics using a CFD tool. Ceruti et al. [8] presented a multidisciplinary design optimisation approach for airships with unconventional configurations. The shape of their airship was based on two semi-ellipsoids whose longitudinal axis ratio can be altered. Zhang et al. [9] proposed a multidisciplinary design optimisation (MDO) methodology for the conceptual design of multi-lobed configuration for high altitude long endurance missions. However, the shape (and hence the aerodynamic characteristics) of the airship were held constant in this study. Ceruti et al. [10] presented a summary of a framework that can be used to optimise the external shape of the multi-lobed airship configuration with a fixed envelope profile of the ellipsoid. The proposed design methodology was based on the parametric design of a tri-lobed envelope to estimate the added mass (AM) using a numerical-based approach and investigated the effect of AM on the performance of the airship during takeoff.

Several studies [11–14] have been carried out by the authors, which have finally resulted in a comprehensive multidisciplinary design optimisation methodology for the conceptual sizing of multi-lobed configuration for stratospheric applications. These studies focused extensively on the parametric design of each component of the airship to achieve the optimum system design for the given mission requirements. The present study proposed a detailed methodology for carrying out the parametric design of multi-lobed hybrid airships.

In an airship, the envelope is the most essential and integral component that affects the aerodynamic performance and weight estimation. Several past studies [15–20] have focused on aerodynamics-based shape optimisation to reduce the drag of the envelope. To perform shape optimisation, each component of the airship should be parameterised with the least number of design variables.

Parametric design is a process of creating and modifying engineering designs using a set of predetermined parameters i.e. design variables. Parametric design has become hugely popular in the field of engineering because it provides an enormous amount of flexibility in the design process to achieve an efficient system design. In aircraft design, a parametric design approach can be used to build and vary the design of the aircraft using open-source or commercially available computer-aided design (CAD) software like *FreeCAD*, *OpenVSP*, *CATIA*, and *Blender*.

To construct a parametric design of an aircraft using CAD, the designer should first fix the parameters that describe the complete geometry of the aircraft. These parameters can usually be the shape and size of the fuselage, the selection of aerofoil and the wing geometry, engine size and location, and other factors that influences the efficiency and appearance of the aircraft.

After the parameters have been fixed, one can use CAD software to create a model of the aircraft using these parameters. Then the user can then change or vary the values of the parameters to see how

it affects the overall design of the aircraft. For example, they can change the wing geometry to check how it influences the aircraft's lift and drag coefficients or they can change the engine size to see how it affects the aircraft's thrust and fuel efficiency.

In this paper, we present a methodology for carrying out the parametric design of multi-lobed hybrid air vehicles (HLAV) using a similar approach. HLAVs, known as heavy lift air vehicles, are a type of aircraft that combine the lift and propulsion capabilities of both fixed-wing and rotary-wing aircraft. They are designed to be highly versatile and able to perform a wide range of missions, including vertical take-off and landing (VTOL) and hovering flight. One of the key differences is the type of lift used by aircraft and airships. Aircraft are typically designed to generate lift using wings whereas airships generate lift using buoyancy provided by a lighter-than-air (LTA) gas such as Helium.

Another key difference is the influence of the aircraft's efficiency and appearance; aircraft generate thrust using one or more engines, whereas airships are powered by a combination of engines and propellers, reducing carbon emission and being greener than other types of transport.

These differences in lift and thrust generation affect the parameters used in the parametric design processes, e.g. the buoyancy control techniques and added mass computations. Overall, this parametric approach is proposed to be an effective way to optimise the stability and performance of the multi-lobed hybrid air vehicles and also reduce the cost and time of the design process.

2.0 Parameterisation of envelope geometry

The airship envelope is the largest component and directly affects the drag acting on it during flight and, hence energy demand. The most challenging task in the design process of an airship is the selection of a suitable envelope profile which has a significant impact on drag generation. As a result, several low-drag shapes have been proposed across the literature [21–24]. A robust shape generation algorithm is required to parameterise the shape of the envelope of an HLAV. The shape generation algorithm allows the optimiser during the design optimisation process to choose an appropriate shape constrained to the desired characteristics. In the following sub-section, two of the shape-generation algorithms that are robust and flexible, viz., Gertler Series 58 and Class Shape Transformation are discussed in detail.

2.1 Generation of envelope profile

Any geometric parameterization model should have several desirable characteristics. It should be well-behaved and produce smooth and realistic shapes. It should be mathematically efficient, numerically stable, fast, accurate and consistent. It should require less number of variables to represent a large domain to contain optimum aerodynamic shapes for varying design conditions and constraints. Finally, it should allow the user to define the specification of design parameters such as leading-edge radius, boat-tail angle, and profile closure.

2.1.1 Class shape transformation method

The Class Shape Transformation (CST) parametrisation technique was developed around 15 years ago by Kulfan [25], an aerodynamicist at Boeing. It incorporates a geometric class/shape function transformation technique. The shape of a specified geometry can be defined using Bernstein polynomials representation of the unit shape function [26]. The CST model is an optimisation technique where a shape can be optimised for analysis using a mathematical model. The optimisation is carried out to obtain an optimum and smooth cross-sectional curve of the desired profile. This method is widely used for the shape generation of aerofoils.

In this method, the first step is to convert the x and y coordinates of the given profile into non-dimensional spatial coordinates, which are defined as $\psi = x/L$ and $\zeta = y/L$. Then, the component shape functions are defined as:

$$S_i(\psi) = K_i \psi_i (1 - \psi)^{n-1} \tag{1}$$

Table 1. *CST-shape coefficients*

Profile	A_1	A_2	A_3	A_4	A_5	A_6	A_7	A_8
NPL	0.2719	0.2675	0.2211	0.2336	−0.2719	−0.2675	−0.2211	0.2336
Wang	0.2914	0.2726	0.2613	0.1372	−0.2914	−0.2726	−0.2613	−0.1372
GNVR	0.3622	0.3486	0.3245	0.1963	−0.3622	−0.3486	−0.3245	−0.1963
LOTTE	0.2393	0.2355	0.3579	−0.0295	−0.2393	−0.2355	−0.3579	0.0295
Zhiyuan-1	0.3094	0.3327	0.3033	0.2497	−0.3094	−0.3327	−0.3033	−0.2497
Garg	0.3421	0.3045	0.3045	0.3421	−0.3421	−0.3045	−0.3045	−0.342

K_i is computed using the following expression:

$$K_i = \binom{n}{i} = \frac{n!}{i!(n-i)!} \tag{2}$$

The overall shape function for the upper surface of the given profile is defined as

$$Su(\psi) = \sum_{i=1}^{n} Au_i.S_i(\psi) \tag{3}$$

where Au_i are the shape coefficients that can be determined using the least-square fit to match a specified geometry. Similarly, the lower surface is defined by the equations

$$Sl(\psi) = \sum_{i=1}^{n} Al_i.S_i(\psi) \tag{4}$$

The generatrix of the given profile can be defined by the following expression:

$$\zeta = C_{N_2}^{N_1}(\psi).Su(\psi) + \psi.\Delta\eta_{TE} \tag{5}$$

where $C_{N_2}^{N_1}(\psi) = \psi^{N_1}(1-\psi)^{N_2}$.

To capture the specified shape, one can vary the values of the shape coefficients in such a way that the error between the specified shape and the approximate one defined by the shape generator is minimised. The function for the minimisation can be written as:

$$f(x) = \sum_{i=1}^{n} \left[y(x_i) - y_i \right] \tag{6}$$

where $y(x_i)$ is the value of the y-coordinate derived from the mathematical equations that define the particular envelope profile and y_i is the value of the y-coordinate generated using the shape generator.

The value of shape coefficients that are required to replicate some standard geometries of a single lobed airship envelope using this method is shown in Table 1.

The different combinations of N_1 and N_2 define a variety of geometric shapes like an aerofoil, elliptic aerofoil, biconvex aerofoil, and Sears-Haack body [26]. The value of N_1 and N_2 was fixed to be 0.5 for the airship envelope profile.

2.1.2 Gertler method

Gertler *et al.* [27, 28] formulated a technique to generate a 2-D curve that can be revolved 360° to develop streamlined bodies-of-revolution for the hull design of high-submerged-speed submarines. This method involves five geometrical parameters as shown in Fig. 1, namely, the position of the maximum section (m), the nose radius (R_0), the tail radius (R_1), prismatic coefficient (C_p) (the ratio of the volume of body-of-revolution to the volume of the cylinder which encloses the body), and the fineness ratio (length over diameter ratio, L/D), which can be used to define the shape of streamlined bodies-of-revolution.
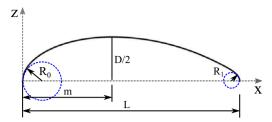
Figure 1. *Design parameters.*

The generatrix of the airship models are derived from a sixth-degree polynomial of the form:

$$y^2 = a_1x + a_2x^2 + a_3x^3 + a_4x^4 + a_5x^5 + a_6x^6 \tag{7}$$

where, the x is the non-dimensional abscissa and y is the non-dimensional ordinate. The non-dimensional offsets X/L vs. Y/D are the same for all the fineness ratios, once the other four geometrical parameters have been fixed.

The shape coefficients $a_1, a_2, \ldots, a_6$ for each profile are determined when the values for the geometrical parameters are assigned. The constraints applicable for the airship envelope are: $y = 0$, when $x = 1$; $y = 1/2$ when $x = m$; and $dy/dx = 0$ when $x = m$. The final equations are obtained in terms of the shape coefficients by satisfying the constraints applicable to the shape of the airship envelope:

$$\begin{cases} a_1 + a_2 + a_3 + \cdots + a_n = 0 \\ a_1m + a_2m^2 + a_3m^3 + \cdots + a_nm^n = \frac{1}{4} \\ a_1 + 2a_2m + 3a_3m^2 + \cdots + na_nm^{n-1} = 0 \end{cases} \tag{8}$$

The radius of curvature for any generatrix may be evaluated from:

$$R = \pm \frac{1}{d^2X/dY^2}\left[1 + \left(\frac{dX}{dY}\right)^2\right]^{3/2} \tag{9}$$

In the dimensionless form, R in Equation (9) can be written as:

$$r = \pm \frac{1}{d^2x/dy^2}\left[1 + \frac{L^2}{D^2}\left(\frac{dx}{dy}\right)^2\right]^{3/2} \tag{10}$$

where, r is the non-dimensional radius, L is the length, and D is the diameter.

The value of dx/dy can be obtained from the successive differentiation of Equation (7) with respect to y:

$$2y = \left(a_1 + 2a_2x + \cdots + na_nx^{n-1}\right)\frac{dx}{dy} \tag{11}$$

and

$$2 = \left(a_1 + 2a_2x + \cdots + na_nx^{n-1}\right)\frac{d^2x}{dy^2} + \left(2a_2 + \cdots + n(n-1)a_nx^{n-2}\right)\left(\frac{dx}{dy}\right)^2 \tag{12}$$

When $x = 0$, $dx/dy = 0$ and hence, from Equation (12) we get:

$$\frac{d^2x}{dy^2} = 2a_1^{-1} \qquad \text{if } a_1 \neq 0 \tag{13}$$

Substituting the value of d^2x/dy^2 in Equation (10), we get:

$$a_1 = 2r_0 \tag{14}$$

where r_0 is the radius of curvature at the nose. If $a_1 = 0$, the body will have a pointed nose ($r_0 = 0$). Hence, Equation (14) is valid for both cases, i.e. $a_1 \neq 0$ or $a_1 = 0$.

Table 2. *Gertler shape coefficients*

Profile	a_1	a_2	a_3	a_4	a_5	a_6
NPL	1.1772	−0.8684	−3.2776	6.9240	−5.5776	1.6227
Wang	1.1999	−0.9065	−2.9418	5.5992	−4.5463	1.5956
GNVR	1.1999	−1.3688	−0.1729	−0.4114	1.1765	−0.4233
LOTTE	1.1518	−5.6907	27.4705	−61.8309	58.4542	−19.5549
Zhiyuan-1	0.6731	4.1778	−22.2435	40.6395	−34.1233	10.8764
Garg	0.9233	1.6775	−14.3812	30.1481	−27.5582	9.1907

Similarly, when $x = 1$, $y = 0$ and from Equation (11) $dx/dy = 0$, unless

$$a_1 + 2a_2 + \cdots + na_n = 0 \tag{15}$$

Hence, Equations (10) and (12) give

$$a_1 + 2a_2 + \cdots + na_n = -2r_1 \tag{16}$$

where r_1 is the radius of curvature at the tail.

The positive sign is taken in Equation (14) and the negative in Equation (16) because r_0 and r_1 are the positive values. a_1 is the slope of the sectional-area curve at $x = 0$, and hence, is positive. Similarly, $a_1 + 2a_2 + \cdots + na_n$ is the slope of the sectional-area curve at $x = 1$, and hence, is negative.

The volume of the envelope (V_{env}) can be expressed as:

$$V_{env} = \int_0^1 \pi Y^2 dX = \pi D^2 L \int_0^1 y^2 dx \tag{17}$$

Substituting for y^2 from Equation (7), we get

$$\frac{1}{2}a_1 + \frac{1}{3}a_2 + \cdots + \frac{n+1}{a_n} = \frac{1}{4}C_p \tag{18}$$

The formulated linear equations (Equations (8), (14), (16), and (18)) can be represented in a matrix form as:

$$AY = B \tag{19}$$

$$
\begin{bmatrix}
1 & 1 & 1 & 1 & 1 & 1 \\
1 & 0 & 0 & 0 & 0 & 0 \\
1 & 2 & 3 & 4 & 5 & 6 \\
m & m^2 & m^3 & m^4 & m^5 & m^6 \\
1 & 2m & 3m^2 & 4m^3 & 5m^4 & 6m^5 \\
\dfrac{1}{2} & \dfrac{1}{3} & \dfrac{1}{4} & \dfrac{1}{5} & \dfrac{1}{6} & \dfrac{1}{7}
\end{bmatrix}
\begin{bmatrix}
a_1 \\ a_2 \\ a_3 \\ a_4 \\ a_5 \\ a_6
\end{bmatrix}
=
\begin{bmatrix}
0 \\ 2r_0 \\ -2r_1 \\ \dfrac{1}{4} \\ 0 \\ \dfrac{1}{4}C_p
\end{bmatrix}
\tag{20}
$$

By solving these six linear equations simultaneously, we can obtain the value for six shape coefficients a_1, a_2, a_3, a_4, a_5, and a_6 for the given geometrical parameters.

The final equation for the airship envelope shape can be written as:

$$y(x) = D \sqrt{a_1 \left(\frac{x}{L}\right) + a_2 \left(\frac{x}{L}\right)^2 + a_3 \left(\frac{x}{L}\right)^3 + a_4 \left(\frac{x}{L}\right)^4 + a_5 \left(\frac{x}{L}\right)^5 + a_6 \left(\frac{x}{L}\right)^6} \tag{21}$$

To obtain the final envelope surface, the curve generated from Equation (21) is revolved around the desired axis to produce the axisymmetric shape of the body. The multi-lobed shape can be considered

Table 3. Gertler design parameters

Profile	m	R_0	R_1	C_p	l/d
NPL	0.4319	0.5886	0.4248	0.6667	4.0000
Wang	0.4040	0.6000	0.1000	0.6100	3.8590
GNVR	0.4143	0.5999	0.1762	0.6163	3.0500
LOTTE	0.4502	0.5759	0.1000	0.5170	3.9019
Zhiyuan-1	0.4193	0.3306	0.2500	0.6489	3.2592
Garg	0.5001	0.4616	0.4601	0.7000	3.2093

Figure 2. Standard envelope profile generated using CST and Gertler method.

as several conventional bodies. A detailed description of the standard envelope profiles represented in Table 2 is given in the 6.

The shape coefficients for standard envelope profiles obtained through Gertler's methods are presented in Table 2. Table 3 shows the list of design parameters obtained from the Gertler-shape generator for standard envelope profiles.

Figure 2 shows that the standard envelope profiles can be generated using CST and Gertler's method. The CST method is more flexible than Gertler's method because the latter method will fail to follow the target curve with a sharp trailing edge as shown in Fig. 2(d).

Table 4. *Comparion between classical method and Gertler's method*

Comparison		Volume (m³)	Error(%)
Reference (24)		254,053	—
Classical approach	$\left(V_{env} = \pi \int_0^1 y^2 dx\right)$	254,060	0.0028
Gertler's method		254,091	0.015

2.2 Estimation of multi-lobed envelope volume

There are many methods that can be found in the existing literature to estimate the volume of the envelope of conventional and unconventional airship geometries. The generatrix for the envelope profile can be generated using the CST method as discussed in Section 2.1.1 or Gertler's method (refer to Section 2.1.2). From the curve defining the profile of the envelope, the surface area and volume can be estimated using the classical approach. The volume of the envelope (V_{env}) with axisymmetric body of revolution is given as:

$$V_{env} = \pi \int_0^1 y^2 dx \tag{22}$$

where y represents the y-coordinates of the given profile generated using shape generators.

The surface area of the envelope is calculated as:

$$S_{env} = 2\pi \int_0^1 y \left[1 + \left(\frac{dy}{dx}\right)^2\right]^{1/2} dx \tag{23}$$

The volume of an airship with the axisymmetric body of revolution can also be estimated through Gertler's method using the following expression:

$$V_{env} = \frac{\pi L D^2 C_p}{4} \tag{24}$$

where L is the length of the envelope, D is the diameter of the envelope, and C_p is the prismatic coefficient.

Table 4 shows the difference in the value of envelope volume computed using the classical and Gertler's method for the *NPL* envelope profile. The classical method is the most convenient method to estimate the volume and surface area for a given generatrix of any profile. Estimation of the envelope volume for a multi-lobed airship involved deduction of the volume of intersection, which is not a straightforward task. To find the volume of a multi-lobed envelope, the intersection volume between the lobes must be calculated. By subtracting the intersection volume from the volume of the lobes, the total volume of the multi-lobed envelope can be calculated. Similarly, the estimation of the wetted surface area of a multi-lobed envelope is a non-trivial task. It is a difficult procedure to calculate the wetted surface area from the surface area of the lobes shown in Equation (23). To compute the wetted surface area, the elemental approach is one of the easiest approaches in which the envelope will be divided into elements. The area of each element will be calculated from its x, y and z coordinates.

The present study compares two different methods to estimate the intersection volume between the lobes. The first method is based on the Monte Carlo method. The latter is based on an analytical approach developed by the authors. In the Monte Carlo method, a random number of points are generated into a domain, viz., a box placed at the intersection of two lobes. All the random points must be checked whether they belong to the intersection or not. From the volume of the defined box, the number of points falling into the intersection, and the total number of generated points, the approximate volume of the intersection between the lobes can be estimated. The volume of the envelope computed by both methods is in good agreement with each other; however, the Monte Carlo method was far more computationally expensive. A comparison between the two methods was carried out for 100 different geometries of tri-lobed envelopes, whose geometry parameters shown in Fig. 3 and 4 were varied.
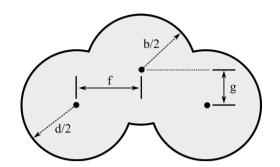
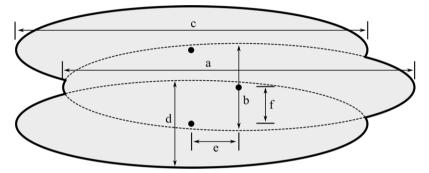***Figure 3.*** *Multi-lobed envelope geometry (front view).*

Figure 4. *Multi-lobed envelope geometry (top view).*

For the implementation of the Monto Carlo method and analytical method, the ellipsoid was chosen as a base profile for each lobe. The geometry function is based on the ellipsoid equation (ellipsoid rotated about the z-axis by angle θ):

$$\frac{\left[(x - x_0)\cos(\theta) + (y - y_0)\sin(\theta)\right]^2}{a^2} + \frac{\left[(x - x_0)\sin(\theta) + (y - y_0)\cos(\theta)\right]^2}{b^2} + \frac{[z - z_0]}{c^2} = 1 \quad (25)$$

In a simple form, it can be defined as

$$x_e + y_e + z_e = 1 \quad (26)$$

The function shown in Equation (25) is to find the randomly generated points belonging to the ellipsoid (it does if Equation (26) is $<= 1$).

In the analytical method, the airship envelope is divided into the number of segments in the longitudinal direction as shown in Fig. 5. Thereafter, the segments which fall inside the intersection volume are taken into consideration. The area of each segment is calculated using geometrical consideration shown in Fig. 6. Then the average area is calculated from the area of each segment in the intersection region. So, multiplying the average area by the length of the intersection defined by X will provide a nearly accurate volume of the intersection between the lobes.

The section volume between the lobes is expressed as:

$$V_{sec} = \text{Average area} \times \text{Length of intersection} = \left(\frac{sum(A_1 : A_n)}{n}\right) \times X \quad (27)$$

where $A_1, A_2, A_3, \ldots, A_n$ is the cross-sectional area of segments in the intersection region and n represents the number of segments.

The total volume of the multi-lobed envelope can be written as:

$$V_{env} = \sum_{i=1}^{N} V_{lobe} - N_I \times V_{sec} \quad (28)$$
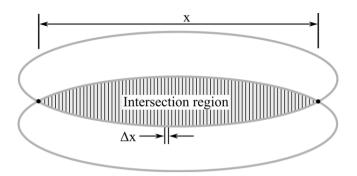
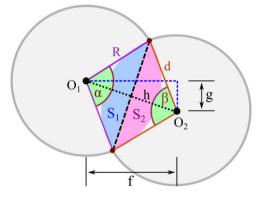**Figure 5.** *Volume of intersection between the lobes.*

Figure 6. *Area of intersection between lobes.*

where N represents the number of lobes and N_I represents the number of intersection regions. For double- and tri-lobed envelopes, the number of intersection regions equals one and two, respectively.

To determine the area of segments in the intersection region, from the cosine rule, we get:

$$\alpha = 2(\cos^{-1}((R^2 + h^2 - d^2)/(2Rh))) \tag{29}$$

$$\beta = 2(\cos^{-1}((d^2 + h^2 - R^2)/(2dh))) \tag{30}$$

In general, the area of a segment between two circles with a radius 'r' is defined as

$$A_{segment} = A_{sector} - A_{triangle} = \left(\frac{\theta}{2}r\right) - \left(\frac{1}{2}r^2 \sin\theta\right) \tag{31}$$

Therefore, the area of segment S_1 and S_2 shown in Fig. 6 can be expressed as:

$$S_1 = \frac{1}{2}d^2(\beta - \sin(\beta)) \tag{32}$$

$$S_2 = \frac{1}{2}R^2(\alpha - \sin(\alpha)) \tag{33}$$

From the given data of envelope volume (fixed to be $V_{env} = 10,000m^3$), the x and y data points that represent the envelope profile and geometry dimensions are generated by back-and-forth calculations for four standard profiles, viz., *Ellipsoid*, *NPL*, *Wang*, and *Zhiyuan-1* to compare the difference in the volume estimation between the proposed analytical method and CAD software. Table 5 represents the difference in the estimation of the volume using the analytical method. The *x*, *y* and other dimension data obtained from the analytical method were used to create the 3D geometry in CAD software.

Table 5. *Comparion of envelope volume* (m^3) *between analytical method and CAD*

Profile	Analytical (m^3)	CAD (m^3)	Error
Ellipsoid		9,972	0.0028
NPL		9,987	0.0013
Wang		9,989	0.0011
GNVR	10,000	9,957	0.0043
Zhiyuan-1		9,989	0.0011
Garg		9,942	0.0058

Figure 7. *Equivalent ellipsoid (reproduced from Ref. (29)).*

For an unconventional airship configuration, it is difficult to determine the exact planform area and wetted area of the envelope. However, it can be approximated by an equivalent shape of an ellipsoid as shown in Fig. 7.

The approximate planform area and wetted area of the envelope can be estimated analytically using the method proposed by Carichner and Nicolai [29]. The wetted area of the multi-lobed envelope is estimated using the Equations (34)–(37).

$$S_{area} = \pi \left((L^p W_{eq}^p + L^p ht^p + W_{eq}^p ht^p) \right) \tag{34}$$

where $p = 1.6075$

$$S_{wetted} = \left(P_{lobes}/P_{ellipse} \right) S_{area} \tag{35}$$

where

$$P_{ellipse} = \pi \left[3(a+b) - \sqrt{10ab + 3(a^2 + b^2)} \right] \tag{36}$$

$$P_{lobes} = N_{lobes} \left(2\pi R \right) - 4 \left(L_{arc} \right) \tag{37}$$

where R is the radius of a lobe and L_{arc} is the arc length of a segment (red-dashed lines) between the lobes shown in Fig. 8.

From the length (L), equivalent width (W_{eq}), and height (ht) of the envelope, the wetted surface area (S_{wetted}) of the tri-lobed envelope is calculated by multiplying the surface area of the equivalent ellipsoid (S_{area}) assuming the shape of a scalene ellipsoid by the ratio of the perimeter of lobes to the perimeter of the ellipse ($P_{lobes}/P_{ellipse}$) shown in Fig. 9.

2.3 Design parameters

The design variables consist of parameters whose values are varied to describe the envelope geometry, size and layout of fins and solar panel layout. The number of design variables depends on the configuration of the airship, viz., conventional and unconventional. The conventional design represents an airship with the axisymmetric body of revolution as shown in Fig. 10(a). The unconventional design represents
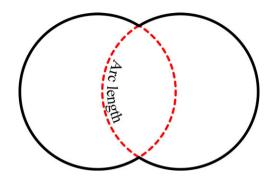
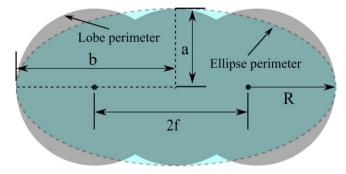**Figure 8.** *Schematic of arc length of a segment.*

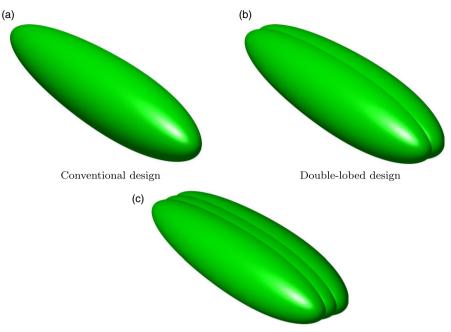**Figure 9.** *Cross-section of the tri-lobed envelope (reproduced from Ref. (29)).*

an airship with a non-axisymmetric body of revolution as shown in Fig. 10(b) and (c). To parameterise the geometry of a conventional airship including envelope, fins and solar panels, 14 (using the Gertler Series 58 Shape Generator for envelope geometry explained in the Section 2.1.2) or 17 (using the Class Shape Transformation (CST) method explained in the Section 2.1.1 for envelope geometry) design variables are required. the first 5 of which are related to the geometry of the envelope, and the next 4 are related to the length of the airship and the layout of the solar array. The last five variables are related to the fin design. In the case of an unconventional airship, viz., multi-lobed dynastat, 18 design variables are required.

2.4 Multi-lobed envelope geometry

Apart from the shape variables that define the profile of a lobe of the tri-lobed envelope, the geometry of the tri-lobed envelope is defined by four design variables such as length of the envelope, (L), the fraction of distance of outer lobes position with respect to central lobe in the longitudinal direction, i.e. along the length of the body, I, the fraction of distance of outer lobes position with respect to central lobe in the lateral direction, (f), and the fraction of distance of outer lobes position with respect to central lobe in the vertical direction, (g). The design variables that define the envelope geometry and layout of the solar array over the surface of the tri-lobed envelope are geometrically explained in Fig. 11.

2.5 Solar array model

A model based on an elemental approach has been developed for the generation of the solar array over the surface of the envelope and estimation of the area of the solar array for the multi-lobed airship. The starting and ending point for the array are decided from the length of the airship. The surface of the envelope between the starting and ending point of the array is divided into $[(m\text{-}1)\times(n\text{-}1)]$ rectangular

(a)

(b)

Conventional design

Double-lobed design

(c)

Tri-lobed design

Figure 10. *Airship geometry.*

(a)

θ_{array}
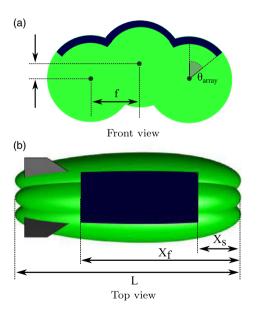
f

Front view

(b)

X_s

X_f

L

Top view

Figure 11. *Trilobed envelope geometry.*

grids as shown in Fig. 12. For any element of the grid, length ($\vec{dl}$) and width ($\vec{db}$) vectors can be expressed in terms of position vector ($\vec{r}$) as:

$$\vec{dl}_{ij} = \vec{r}_{i,j+1} - \vec{r}_{i,j} \tag{38}$$

$$\vec{db}_{ij} = \vec{r}_{i+1,j} - \vec{r}_{i,j} \tag{39}$$

Figure 12. *Schematic of solar array grid on the envelope.*

Figure 13. *Geometry of the solar array.*

For a conventional airship with the axisymmetric body of revolution, the solar array model is very simple without any geometrical complications. But for the multi-lobed configurations, there are several geometrical complications because of the orientation of the lobes with respect to one another. The solar array grid has to be generated over the surface of the envelope to estimate the energy available based on the orientation of each element of the generated grid with respect to the Sun vector. In the multi-lobed configuration, the lobes are merged together based on the value of e, f and g. Hence, it is not simple to generate the grid over the surface. The orientation of the lobes and merging points between the lobes at each section of the envelope have to be calculated using trigonometric relations as shown in Fig. 13.

The entire array model can be parameterised using three design parameters, viz., the starting point of the array (X_s), ending point of the array (X_f) and intended angle of the array (θ_{array}). Figure 14 shows the solar array generation over the conventional and multi-lobed configurations.

2.6 Vehicle sizing and performance model

For a given set of design parameters and operating conditions, a design solution is obtained using an iterative design loop as shown in Fig. 15. The first stage in the design process involves the selection of the appropriate envelope profile and sizing of the envelope in order to produce the required lift. In this proposed methodology, the shape of the envelope profile and envelope geometry can be varied according to the mission requirements and constraints.
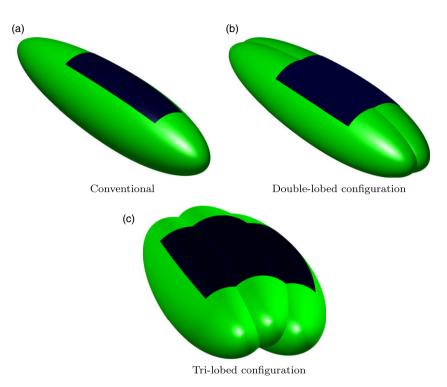
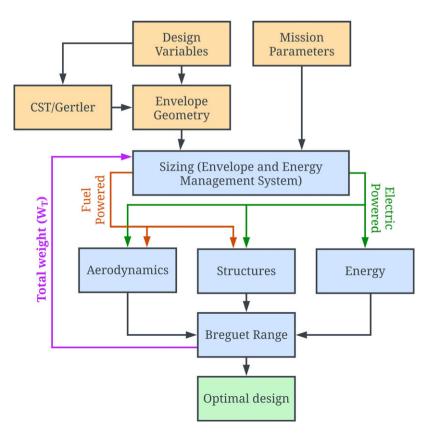*Figure 14. Solar array over conventional and multi-lobed configurations.*

Figure 15. Schematic of vehicle design.

Many existing studies have limited the design space to a fixed envelope profile and geometry for the initial sizing. To select the ideal shape of an airship, several factors need to be considered including the size and mass of the airship, the materials it is made from, the lift (static and dynamic) and drag forces acting on the airship and the desired performance characteristics. One of the best approaches in selecting the ideal shape would be to use CFD simulations to model the flow of air around the airship and optimise the shape to minimise the drag and maximise the aerodynamic efficiency (C_L/C_D). The simplest approach might be to use empirical data and mathematical models to predict the lift and drag forces acting on the airship and optimise the shape based on these predictions. There are many factors that can affect the aerodynamic performance of an airship, including the size and shape of the envelope, the size and layout of the tail surfaces, the selection of the propellers and the position and orientation of the engines. To obtain the ideal shape, all of these factors must be considered during the optimisation to meet the desired performance goals. It is important to note that the ideal shape for an airship will depend on the specific design constraints and performance goals of the airship.

Wind tunnel testing is one of the standard procedures to optimise the design of an airship body and is also a good means for accurately measuring the aerodynamic characteristics and moment. The larger size and high Reynolds number at low speed enhance the complexity of measuring the aerodynamic forces and moments using a wind tunnel [30].

Payload weight and power requirement are the two key parameters that drive the sizing process of any aircraft. For an airship, the maximum range and maximum cruise altitude define the required envelope volume and total mass. The choice of range decides the fuel requirement for conventional fuel-powered airships and the size of the energy management system for electric-powered airships. Maximum cruise altitude has a significant impact on the selection of envelope material and the choice of internal structures to withstand the required pressure difference that needs to be maintained at that high altitude.

The total mass of the airship can be derived by estimating the mass of each sub-system of the vehicle. There are a set of empirical relations to estimate the mass of sub-systems of airships presented by Carichner and Nicolai based on existing airship models in [29]. The major mass contribution comes from the hull of the airship. The hull mass includes envelope mass, tail mass and ballonet mass. The envelope mass is calculated from the estimation of surface area, maximum stress requirement and envelope material density. The selection of envelope material plays a significant role in mass estimation. Ballonet mass estimation depends on the pressure differential required to maintain the required buoyancy and operating altitude. The tail mass is calculated from the material properties, internal frames and surface area of the fins.

The value of the total mass of the airship and the aerodynamic characteristics data are then passed into the Breguet Range Equation to obtain the revised gross weight. The process is iterated until a solution is found.

In this study, we have focused on the application of open-source software currently available to the public and based on the existing literature. The complete design and optimisation framework involves multiple disciplines that can be developed using publicly available open-source software. Figure 16 shows the interface between the software to achieve an optimal design using the parametric design approach.

With the given design parameters and specified mission requirements, Fig. 16 gives an idea of how a model undergoes the mentioned processes such as CAD modeling, meshing and analysis to generate an optimal design output.

By using the initial design parameters, the first step in the design process is to create a CAD model. CAD modeling is an important aspect of parametric design as it allows designers to make detailed, accurate representations of the model's structure and components. For this *FreeCAD* or *SALOME* can be used for modeling as they are open-source and completely free to use. After finalising the CAD model, it undergoes the meshing process.

Meshing is the process of dividing a continuous physical space into discrete elements, such as points, lines or surfaces. In parametric design, meshing is often used to represent a design model as a collection of interconnected elements. This allows designers to analyse and optimise the design using computational techniques, such as FEA or CFD.
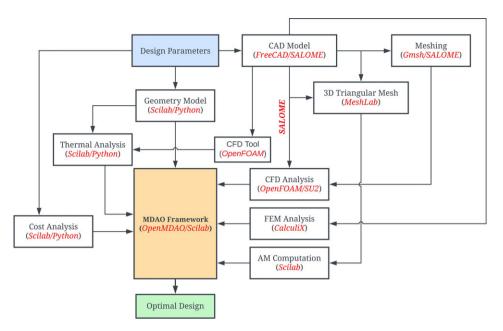
Figure 16. *Design framework based on open-source software(s).*

To save time, *SALOME* can do both modeling and meshing and later can be exported for analysis. Alternatively, the CAD model from *FreeCAD* can be imported into other open-source software, e.g. *Gmsh* and *MeshLab* for the meshing.

The analysis and simulation methods can be classified into CFD, FEM and thermal analysis. Computational fluid dynamics (CFD) is a numerical method used to simulate and analyse the flow of fluids, such as gases and liquids, through and around objects. It involves solving mathematical equations that describe the behaviour of fluids to predict the flow patterns, pressures and temperatures in a given system. To achieve this, software like *OpenFOAM* or *SU2* can be used for studying the flow properties around the body, improving its aerodynamics of it, and getting an optimised shape reducing the drag and improving the lift.

The FEM is a numerical method used to solve problems involving the behaviour of structures and materials under load. It involves dividing the structure or material into smaller, simpler shapes called 'finite elements' and solving equations that describe the behaviour of each element. FEM is often used in conjunction with CFD to analyse the thermal behaviour of structures and materials, as well as their structural integrity. Software such as *CalculiX* is used for static structural analysis.

Thermal analysis is a subset of CFD that focuses on predicting and analysing the temperature distribution in a system. It is often used to design and optimise heat transfer systems, predict the performance of cooling systems, and identify areas of high-temperature gradients or thermal stress. This type of analysis can be simulated in the CFD tool or in *Scilab/Python* to get heat transfer results by solving the simultaneous energy equations.

For LTA systems such as airships, Added Mass (AM) is one of the important parameters during accelerated flight. AM is the mass of air that an airship displaces as it moves through the air. This consideration is very important in the design and performance of the body as it affects performance, stability and manoeuverability. To compute the AM of an airship, the shape and dimensions of the airship must be known, as well as the density of the air through which the airship will be moving. To calculate the AM, the meshed model is imported into *Scilab/Python* platform.

The initial and operating cost of an airship is also an important consideration, apart from the design and sizing. This depends on several factors such as size, material, the technology used and the operating environment of the system. *Scilab/Python* can be used for doing such tasks.
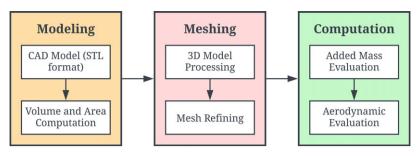
Figure 17. *Procedure to compute added mass (adapted from Ref. (10)).*

Finally, after sorting out all the workflow processes, the model and the supporting data are inserted into the MDOA (model, design, optimise, and analyse) framework, which uses a set of algorithms to produce an optimal design that fits in every aspect. It is a systematic approach to designing a product. This could be done using *Scilab/Python* by creating a machine learning model, which processes the given data to produce an optimised product.

3.0 Added mass computation

This section deals with investigating the effect of multi-lobed envelope geometries on the added mass computation. The term "added mass" refers to the inertia of the mass of the fluid displaced by the body. The added mass term plays a significant role in the performance and dynamics of the vehicle when the mass of the fluid displaced is larger than the mass of the vehicle itself. The added mass concept is related to the acceleration or deceleration of the body, which is immersed in a fluid. In this study, Boundary Element Method (BEM) was used to estimate the added mass components. The detailed description and the mathematical formulation of the BEM to compute the added mass matrix of a body moving in a fluid can be found in [31, 32].

Multi-lobed geometry parameterisation is a function of envelope shape that affects the volume and surface area. For a given volume, the size of the airship can be different based on the envelope profile. The proposed method uses CAD software, meshing software and numerical computing software for added mass computation as shown in Fig. 17.

The developed methodology to compute the added mass of a given geometry involves three steps. Firstly, the geometry has to be parameterised and modeled using open-source or any commercial-based CAD software. Ceruti et al. [10] have used open-source software, viz., *FreeCAD* in one of their studies to model the required geometry. In that study, the shape of the envelope was fixed to be an ellipsoid. Figure 18 shows the STL format model generated using *Autodesk* Fusion 360. Following the modeling of geometry, meshing has to be done to discretise the complex structure into small triangular elements. In the present study, the open-source software, viz., *MeshLab* is used for processing and editing 3D triangular meshes. Finally, the meshed model in STL file format is passed on to the added mass computation algorithm developed in a numeric computing platform based on BEM.

To test the developed algorithm, two cases with dimensions as same as the reference study [32] were taken into consideration. The first case was a sphere with a radius of 1 m and 3,192 triangles, and the second was an ellipsoid with a semi-major axis (a) of 4 m, a semi-minor axis (b) of 1 m, and 3,960 triangles. The results are in good agreement with the reference study as shown in Table 6.

For a given volume of $10,000 \text{m}^3$, four different tri-lobed models were developed based on the standard envelope profiles, viz., *Ellipsoid*, *NPL*, *Zhiyuan*, and *Wang*. Following the approach described in the methodology, added mass matrices were computed. AM_{11} term is the contribution of AM along the longitudinal axis that resists the motion of the object immersed in a fluid while it is accelerating or decelerating. In the equations of motion, this term must be included to account for the drag due to the

Table 6. *Data comparison between reference and the present study*

Model		AM_x	AM_y	AM_z
	Reference (32)	0.478	0.478	0.478
Sphere; Radius = 1m; 3,192 triangles	Present study	0.480	0.480	0.478
	Error %	**0.4**	**0.4**	**Nil**
	Reference [32]	0.0808	0.803	0.803
Ellipsoid; a = 4 m; b = c = 1m; 3,960 triangles	Present study	0.0795	0.807	0.807
	Error %	**1.6**	**0.5**	**0.5**

Figure 18. *STL model for added mass computation.*

Table 7. *AM contribution along the longitudinal axis*

Reference volume (m³)	Lobes profile	AM_{11}
	Ellipsoid	0.0848
	NPL	0.1150
10000	*Wang*	0.1256
	GNVR	0.1706
	Zhiyuan-1	0.1528
	Garg	0.1573

displacement of mass during the motion of the vehicle. The AM_{11} data of the four different models are given in Table 7.

4.0 Tail design and sizing

The tail is an important component of the airship that provides control and stability to the airship. The horizontal tail provides longitudinal stability and pitch manoeuver, whilst the vertical tail governs the lateral-directional stability, roll and yaw characteristics. The tail design is a significant element in the airship design process which affects the total weight estimation. The initial sizing of the tail can be obtained through the determination of the tail moment arm (i.e. the distance between the front quarter of the tail mean aerodynamic chord, i.e. MAC, and the airship centre of gravity, i.e. *c.g.*). But it is not an easy approach, because the *c.g.* of an airship has to be derived from the exact weight and relative position of all the components and systems.

Tail sizing has a significant impact on the static and dynamic stability of an airship. The tail of an airship provides stability by creating a moment that opposes any disturbance from the airship's equilibrium state. A larger tail size generally provides greater static stability, as it creates a larger moment arm and therefore greater stabilising force. Conversely, a smaller tail size can result in less static stability, which can make the airship more manoeuverable but also less stable in certain flight conditions. A properly sized tail can contribute to positive dynamic stability by dampening out oscillations in pitch and yaw. A tail that is too small can lead to a lack of damping, which can result in unstable or uncontrollable oscillations. In summary, tail sizing plays a critical role in determining the stability of an airship. While larger tails generally provide greater static and dynamic stability, the optimum tail size depends on a variety of factors, including the aircraft's weight, size and intended use.

In general, airships are directionally unstable because of their undersized fins [33]. Fins have a significant effect on the aerodynamics of airships as well as their stability and control characteristics. Due to the limitation of the strength of the envelope materials, the required size of fins cannot be employed. This results in the poor generation of restoring forces and moments to counteract the components that destabilise the airship. Another reason for being unstable is that the airships operate at low Mach number ($M < 0.2$) and Reynolds number. Several methodologies are available for the sizing of hybrid airships, minimal importance is given to the sizing of fins during the design process. Stability is one of the major concerns of the design of high-altitude airships for station-keeping, to be considered for safety and uninterrupted operations. Static and dynamic stability is directly related to the size of the fins. Hence, the sizing of fins is one of the important elements of the overall design process. Figure 19 shows the forces and moments acting over an airship.

4.1 Tail sizing

At the point of initial sizing, the airship has been sized (estimation of the envelope volume) based on its takeoff gross weight (*TOGW*). A configuration in terms of the number of lobes (N_{lobes}) and fineness
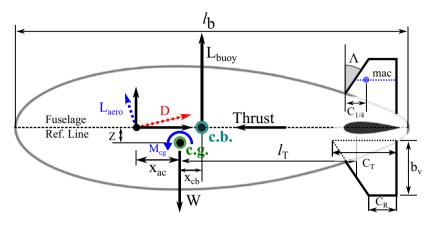
Figure 19. *Forces and moments acting on a buoyant airship.*

ratio (l/d) has also been assumed. For the selected configuration, aerodynamic analysis and components weight estimation need to be performed to estimate the drag and fuel/solar array required to accomplish the mission, the empty weight, and the *c.g.* location. Tail sizing is one of the important phases in the configuration design of airships since it typically accounts for $10 - 14\%$ of the empty weight and 20% of the airship C_{D0}. The initial sizing of the tail fins is carried out using a procedure based on historical data called the tail volume coefficient approach. In the initial design process, the location of *c.g.* and its movement with the change in weight of the airship is unknown. But it is predicted that the *c.g.* will be close to the centre of buoyancy (*c.b.*). From the historical data, the *c.b.* is typically located at 45% of the airship length from the nose, and the moment arm varies between $36 - 43\%$ of the length of the airship. [29] Figure 20 describes the tail sizing procedure given in Ref. (34).

The horizontal tail (C_{HT}) and vertical tail (C_{VT}) coefficients are defined as follows:

$$C_{HT} = \frac{l_{HT} S_{HT}}{l_b V_{env}^{2/3}} \tag{40}$$

$$C_{VT} = \frac{l_{VT} S_{VT}}{l_b V_{env}^{2/3}} \tag{41}$$

where, l_{HT} and l_{VT} are the distance between the *c.g.* and the quarter chord of the tail fin mean aerodynamic centre (m.a.c.), S_{HT} and S_{VT} are the projected planform area of the horizontal and vertical fins, respectively, and l_b is the length of the airship.

The tail volume coefficient is a function of the tail surface area (S_{HT}), and the tail surface area is readily determined using the Equations (40) and (41). From the historical data of existing airships, Carichner and Nicolai [29] estimated the horizontal tail (C_{HT}) and vertical tail (C_{VT}) coefficients as a function of airship volume. From the curve fitting to the historical data, the horizontal and vertical tail volume coefficient as a function of envelope volume is derived as:
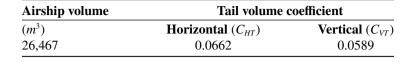
$$C_{HT} = -0.0051x + 0.0717 \tag{42}$$

$$C_{VT} = -0.0049x + 0.0641 \tag{43}$$

where, $x = 10^6$/envelope volume (in ft^3).

For the present study, the reference envelope volume was taken from the solved example of a hybrid airship given in Chapter 12 of Ref. (29). The horizontal and vertical tail volume coefficients for the reference envelope volume are listed in Table 8. From the given airship volume, three different tri-lobed envelope geometry were developed.

Table 8. *Tail volume coefficient*

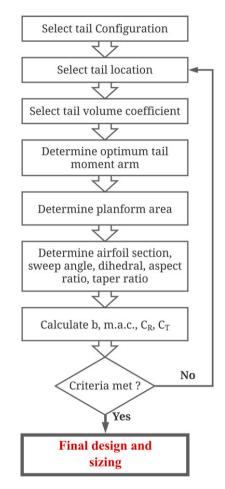| Airship volume	Tail volume coefficient	
(m^3)	**Horizontal** (C_{HT})	**Vertical** (C_{VT})
26,467	0.0662	0.0589

Figure 20. *Tail design procedure (adapted from Ref. (34)).*

4.2 Aft tail configuration

The selection of tail configuration is the first step in the sizing of the tail as shown in Fig. 20. An aft tail has several configurations that are designed to satisfy the design requirements. Each configuration has unique advantages and disadvantages.

Typically, a hybrid airship has four tail surfaces or two pairs of tails. The X-tail configuration shown in Fig. 21(c) has a dihedral angle of 45°, with the advantage of each tail surface contributing to both lateral-directional and longitudinal stability. One more advantage of the X-tail is the reduction in the overall height of the airship. The two important objectives that need to be achieved at the end of the design process of an airship are low weight and low drag. The wetted area of an airship significantly affects the drag and weight.

Y-tail configuration is the best tail configuration for conventional airships from the aerodynamic point of view [29, 35], because it has a lower zero-lift drag coefficient and high lift curve slope than other configurations shown in Fig. 22(b). Next to the Y-tail, the X-tail configuration has the lowest zero-lift
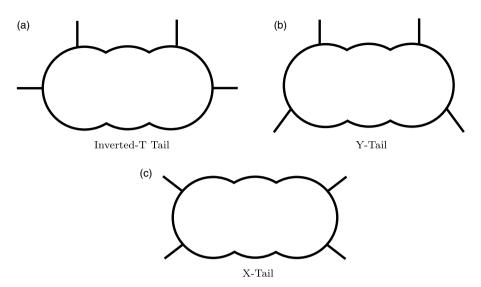
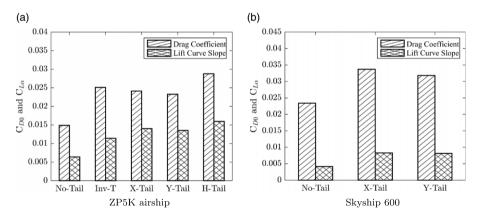**Figure 21.** *Tail configurations for multi-lobed airship.*

Figure 22. *Drag and lift curve characteristics for different tail configuration.*

drag coefficient and high lift curve slope as shown in Fig. 22(a). The suitable tail configuration for the multi-lobed hybrid airship configuration has to be explored by performing the aerodynamics analysis of an airship with different tail configurations.

The second step is to determine the horizontal and vertical tail surface area. The tail surface area can be calculated from:

$$S_{HT} = \frac{C_{HT}l_b V_{env}^{2/3}}{l_{HT}} \tag{44}$$

$$S_{VT} = \frac{C_{VT}l_b V_{env}^{2/3}}{l_{VT}} \tag{45}$$

For the X-tail configuration, the surface area (S_A) of each fin (A_1, A_2, A_3, and A_4) can be obtained from:

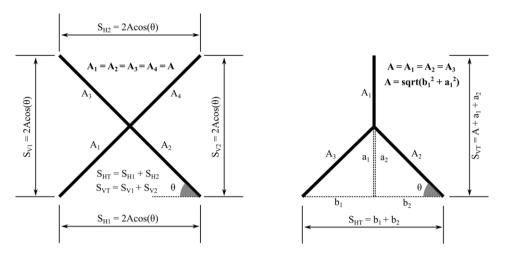$$S_A = \sqrt{\left(\frac{S_{HT}}{4}\right)^2 + \left(\frac{S_{VT}}{4}\right)^2} \tag{46}$$

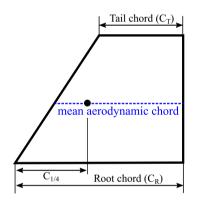**Figure 23.** *Tail geometry and surface area.*

Figure 24. *Tail geometry.*

Similarly, for the Y-tail configuration, the surface area of a fin and the inclination angle are calculated as:

$$S_A = \frac{-\frac{2}{3}S_{VT} + \sqrt{\left(\frac{2}{3}S_{VT}\right)^2 + \frac{4}{3}\left(S_{VT}^2 + S_{HT}^2\right)}}{2} \tag{47}$$

$$\theta = \arccos\left(\frac{S_{HT}}{2S_A}\right) \tag{48}$$

The mean aerodynamic chord shown in Fig. 24 for the tail can be expressed as:

$$MAC = \left(\frac{2}{3}\right)\frac{C_R\left(1 + \lambda + \lambda^2\right)}{1 + \lambda} \tag{49}$$

where, C_R is the root chord of the fin and λ, the tail taper ratio.

Taper ratio is a design parameter of the horizontal and vertical tails similar to the wing of an aircraft which has a significant impact on the overall stability and control, aerodynamic performance, tail aerodynamic efficiency and weight as well as the centre of gravity location. [34] The tail taper ratio is defined as the ratio of the tail tip chord (C_T) to the root chord (C_R). In this study, the tail taper ratio of 0.6 is used. Figure 25 shows the standardised schematic view of fin geometry.
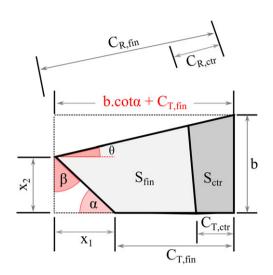
$$\lambda = \frac{C_T}{C_R} \tag{50}$$
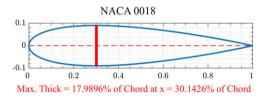
Figure 25. *Schematic view of a Fin.*

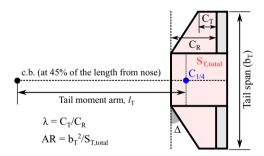**Figure 26.** *Schematic of NACA 0018 aerofoil.*

Figure 27. *Tail surface.*

Airships employ aerofoils operating at a relatively low Re range between 10^4 to 10^6. In the present study, NACA 0018 aerofoil shown in Fig. 26 is used.

Tail layout and the hull-fin interaction have a significant impact on the dynamics (stability and control) of the airship [35]. Tail sizing is not a direct method and has to be refined with the change and progress in the design process. The parameters involved in the sizing of the tail surface shown in Fig. 27 and to estimate its effect on the aerodynamics of a full vehicle are the number of tail pairs (N_{fins}), exposed tail area (S_T), total tail area ($S_T)_{total}$, tail moment arm from *c.b.* to tail (l_T), tail span (b_T), tail aspect ratio (AR_T), tail sweep angle at a maximum thickness (Δ), tail lift curve slope ($C_{L\alpha})_{tail}$, tail dihedral angle (Γ), reference volume (*Vol*) and length of the body (l_b).

In this study, the tail moment arm (l_T) is set to be 40% of the airship length based on the observation of the typical moment arm of existing airships.
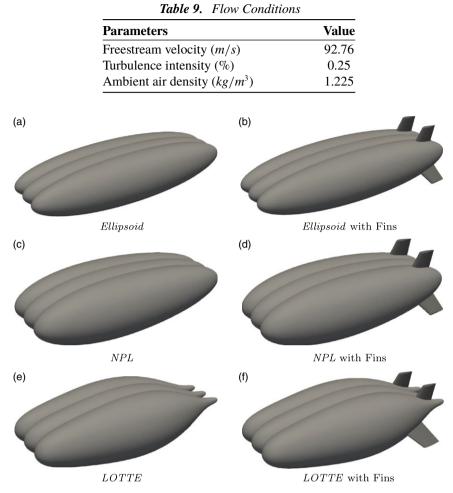
Table 9. *Flow Conditions*

Parameters	Value
Freestream velocity (m/s)	92.76
Turbulence intensity (%)	0.25
Ambient air density (kg/m^3)	1.225

(a) *Ellipsoid*   (b) *Ellipsoid* with Fins

(c) *NPL*   (d) *NPL* with Fins

(e) *LOTTE*   (f) *LOTTE* with Fins

Figure 28. *Tri-lobed geometry with fins.*

4.3 Effect of fins on airship drag

This section carries out a preliminary evaluation of the effects of fin sizing on the overall aerodynamics of a tri-lobed geometry through a series of numerical investigations carried out at subsonic and high Reynolds number flow conditions. The study compares the drag coefficients at zero degrees angle-of-attack for three tri-lobed airship models pertaining to different hull profiles, namely *Ellipsoid*, *LOTTE* and *NPL* tri-lobed models. Figure 28 presents the three-dimensional view of the three tri-lobed hull variants for both bare hull and hull with fin configurations. The three models have been designed using the algorithm mentioned earlier while keeping the same volume across the different variants. Flow similarity across the three variants has been achieved using the same Re under the same Mach number (M) conditions that are $M < 0.3$. Values related to the other parameters associated with the simulated flow conditions are given in Table 9. Fin sizing was accomplished by keeping the volumetric tail coefficient constant at 0.0662 for the horizontal tail and 0.0589 for the vertical tail. Fins for all the models were placed at a distance of 40% from the centre of buoyancy. The latter is located at a distance of 45% location on the central axis of the hull.

4.4 Mesh setup

Mesh was generated using the *snappyHexMesh* tool of *OpenFOAM*. Mesh density was varied according to the flow gradient associated with the geometry. Thus, the mesh was dense closer to the walls,
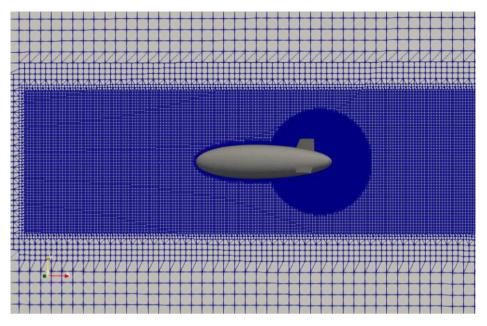
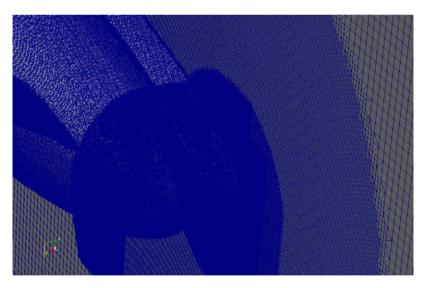***Figure 29.*** *Variable mesh density.*

Figure 30. *Mesh refinement at rear portion.*

followed by a higher density near the rear portion of the hull shown in Fig. 29. Furthermore, to efficiently snap the mesh and capture flow variations pertaining to the curve corresponding to the intersection of the two lobes, the mesh was refined in the region close to this intersection using a spherical refinement volume shown in Fig. 30. The inflation layer shown in Fig. 31 was generated close to the walls to capture flow variations related to the boundary layer of the simulated geometry. This layer was adjusted such that the y^+ was less than 5. Based on these refinements the cell for this particular study ranged between 18 million to 35 million cells with a higher mesh count being used for the hull with fins.

During the simulations, the inlet, outlet and far-field boundaries were assigned the free-stream boundary conditions, whereas the wall was assigned the no-slip boundary condition. After generating the mesh

Table 10. *Geometry data of five different models*

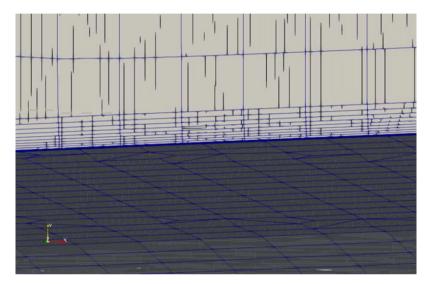| Model	Length (m)	Width (m)	f (m)
Ellipsoid	87.67	28.05	5.26
LOTTE	80.18	32.88	6.16
NPL	75.55	30.22	5.67

Figure 31. *Inflation layer close to the model.*

and defining the boundary conditions, steady-state solutions pertaining to this study were acquired using the *simpleFOAM* solver while making use of the two-equation *SST k-ω* turbulence model for carrying out Reynolds-Averaged Navier-Stokes evaluations. Further details related to the solver setup can be acquired from a previous study carried out using a similar solver setup in [36]. The solver was deemed to have converged upon acquiring a stable, normalised residual of five orders of magnitude.

Preliminary conclusions regarding the aerodynamic effect of fin placement on the scaled-down models of the tri-lobed models of different hull profiles were drawn out by comparing the drag coefficients for these variants at zero degrees angle-of-attack.

4.5 Results and discussions

For the given envelope volume of $V_{env} = 26,476 m^3$, the geometry data are calculated and the values are given in Table 10. The variable f represents the distance between the lobes in the lateral direction.

The values of C_{DV} obtained from CFD simulations for bare hull models and models with fins are shown in Fig. 32.

The outcomes of the CFD simulation for bare hull models and models with fins are given in Table 11.

To investigate the effect of fins on the aerodynamics of multi-lobed airships, numerical simulations were carried out for three different models of the tri-lobed airship with and without fins designed for the same envelope volume. It is interesting to note that there is a difference of $20 - 30\%$ in the volumetric drag coefficient between the bare hull and hull with fins. This study on fin sizing serves as a baseline for the initial sizing of multi-lobed hybrid airships for various applications.

Table 11. *Volumetric drag coefficient*

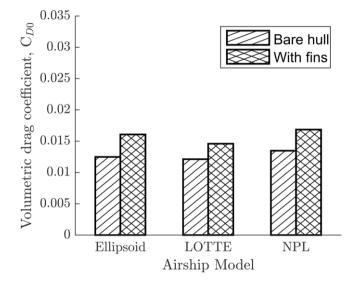| Model	C_{D0} (bare hull)	C_{D0} (with fins)	$\%\Delta C_{D0}$
Ellipsoid	0.01248	0.01607	28.70
LOTTE	0.01212	0.01460	20.50
NPL	0.01348	0.01685	25.01

Figure 32. *Comparison of volumetric drag coefficient.*

5.0 Conclusions

In the present study, a highly robust multi-disciplinary design approach has been developed in terms of geometry parameterisation. The challenging part of the hybrid airship design is the estimation of aerodynamic characteristics of the bare hull and complete configuration including additional lifting surfaces, namely fins, strakes and leading-edge root extension (LERX). The most efficient method to capture the aerodynamics of such complex systems is the application of computational fluid dynamics (CFD). But coupling the CFD solver to the developed methodology poses challenges in terms of computational cost. The most challenging task in using CFD for the computation of aerodynamic forces of the hybrid airship is the validation of the results. There is an acute shortage of sufficient aerodynamic data pertaining to hybrid airships available to the public to carry out solver validation. Since there are no publicly available wind tunnel data for multi-lobed hybrid airships, aerodynamic assertions drawn out from a CFD study can be done merely based on the solver's ability to capture the flow physics associated with conventional airships through the analysis of flow-field visualisation and pressure-velocity flow-field data.

The developed methodology can serve as a conceptual design tool to obtain the size and shape of the multi-lobed envelope, the size and layout of the solar array, the altitude of deployment and mass breakdown in an optimal fashion for any given user requirements and deployment location. It has the capability to give the results of MDO for multi-objective optimisation. The different optimisers can be easily coupled to the method and results can be compared.

Author contributions. Conceptualisation – Manikandan M., Ruchit R. Shah, and Rajkumar S. Pant; Methodology – Manikandan M., and Ruchit R. Shah; Software – Manikandan M., Balbir Singh, and Pughazhendhi Priyan; Validation – Manikandan M., Ruchit R. Shah, and Pughazhendhi Priyan; Writing—original draft preparation – Manikandan M. and Balbir Singh; Writing—review and

editing – Rajkumar S. Pant, Balbir Singh, and Manikandan M.; Supervision – Rajkumar S. Pant. All authors have read and agreed to the published version of the manuscript.

Institutional review. Not applicable.

Informed consent. Not applicable.

Conflicts of interest. The authors declare no conflict of interest.

References

[1] Boyd, R. Performance of hybrid air vehicles, In *40th AIAA Aerospace Sciences Meeting & Exhibit*, p 388, 2002.

[2] Donaldson, A., Simaiakis, I., Lovegren, J., Pyrgiotis, N., Li, L., Dorbian, C. and He, C. Parametric design of low emission hybrid-lift cargo aircraft, In *48th AIAA Aerospace Sciences Meeting Including the New Horizons Forum and Aerospace Exposition*, p 1395, 2010.

[3] Agte, J., Gan, T., Kunzi, F., March, A., Sato, S., Suarez, B. and Yutko, B. Conceptual design of a hybrid lift airship for intra-regional flexible access transport, In *48th AIAA Aerospace Sciences Meeting Including the New Horizons Forum and Aerospace Exposition*, p 1391, 2010.

[4] Carichner, G. and Nicolai, L.M. Hybrids… the airship messiah? In *AIAA Lighter-Than-Air Systems Technology (LTA) Conference*, p 1317, 2013.

[5] Verma, A.R., Sagar, K.K. and Priyadarshi, P. Optimum buoyant and aerodynamic lift for a lifting-body hybrid airship, *J Aircr*, 2014, **51**, (5), pp 1345–1350.

[6] Ceruti, A. and Marzocca, P. Conceptual approach to unconventional airship design and synthesis, *J Aerosp Eng*, 2014, **27**, (6), p 04014035.

[7] Mahzan, M.I. and Muhamad, S. An evolution of hybrid airship vehicle (hav) envelope: Aerodynamics analysis, In *Applied Mechanics and Materials*, vol. 660, pp 498–502. Trans Tech Publ, 2014.

[8] Ceruti, A., Voloshin, V. and Marzocca, P. Heuristic algorithms applied to multidisciplinary design optimization of unconventional airship configuration, *J Aircr*, 2014, **51**, (6), pp 1758–1772.

[9] Zhang, L., Lv, M., Meng, J. and Du, H. Optimization of solar-powered hybrid airship conceptual design. *Aerosp Sci Technol*, 2017, **65**, pp 54–61.

[10] Ceruti, A., Gambacorta, D. and Marzocca, P. Unconventional hybrid airships design optimization accounting for added masses. *Aerosp Sci Technol*, 2018, **72**, pp 164–173.

[11] Manikandan, M. and Pant, R.S. Design optimization of a tri-lobed solar powered stratospheric airship, *Aerosp Sci Technol*, 2019, **91**, pp 255–262.

[12] Manikandan, M. and Pant, R.S. Conceptual design optimization of high-altitude airship having a tri-lobed envelope, In *Advances in Multidisciplinary Analysis and Optimization*, pp 49–61. Springer, 2020.

[13] Manikandan, M. and Pant, R.S. A comparative study of conventional and tri-lobed stratospheric airships, *Aeronaut J*, 2021, **125**, (1290), pp 1434–1466.

[14] Manikandan, M. and Pant, R.S. Multidisciplinary design approach for solar-powered tri-lobed halesa. *Energy Conver Manag*, 2021, **245**, p 114616.

[15] Lutz, T. and Wagner, S. Drag reduction and shape optimization of airship bodies, *J Aircr*, 1998, **35**, (3), pp 345–351.

[16] Wang, X.-l. and Shan, X.-x. Shape optimization of stratosphere airship, *J Aircr*, 2006, **43**, (1), pp 283–286.

[17] Wang, Q.-b., Chen, J.-a., Fu, G.-y. and Duan, D.-p. An approach for shape optimization of stratosphere airships based on multidisciplinary design optimization, *J Zhejiang Univ-Sci A*, 2009, **10**(11), pp 1609–1616.

[18] Alam, M.I. and Pant, R.S. Surrogate based shape optimization of airship envelopes. In *24th AIAA Aerodynamic Decelerator Systems Technology Conference*, p 3393, 2017.

[19] Buckley, H.P., Holt, N., Leinonen, A., Fournier, S. and Zingg, D.W. Preliminary design of a solar-powered hybrid airship, *J Aircr*, 2020, **57**, (2), pp 256–267.

[20] Manikandan, M. and Pant, R.S. Surrogate based aerodynamic shape optimization of tri-lobed hybrid airship envelope, In *AIAA AVIATION Forum and Exposition*, 2021.

[21] Wang, Q., Chen, J., Fu, G., Duan, D. and Zhao, H. A methodology for optimisation design and analysis of stratosphere airship, *Aeronaut J*, 2009, **113**, (1146), pp 533–540.

[22] Ram, C.V. and Pant, R.S. Multidisciplinary shape optimization of aerostat envelopes. *J Aircr*, 2010, **47**(3), pp 1073–1076.

[23] Garg, A., Burnwal, S., Pallapothu, A., Alawa, R. and Ghosh, A. Solar panel area estimation and optimization for geostationary stratospheric airships, In *11th AIAA Aviation Technology, Integration, and Operations (ATIO) Conference, including the AIAA Balloon Systems Conference and 19th AIAA Lighter-Than*, p 6974, 2011.

[24] Liang, H., Zhu, M., Guo, X. and Zheng, Z. Conceptual design optimization of high altitude airship in concurrent subspace optimization, In *50th AIAA Aerospace Sciences Meeting Including the New Horizons Forum and Aerospace Exposition*, p 1180, 2012.

[25] Kulfan, B.M. Universal parametric geometry representation method, *J Aircr*, 2008, **45**, (1), pp 142–158.

[26] Kulfan, B. and Bussoletti, J. Fundamental parameteric geometry representations for aircraft component shapes, In *11th AIAA/ISSMO Multidisciplinary Analysis and Optimization Conference*, p 6948, 2006.

[27] Gertler, M. *Resistance Experiments on a Systematic Series of Streamlined Bodies of Revolution: For Application to the Design of High-Speed Submarines*. Navy Department, David W. Taylor Model Basin, 1950.

[28] Landweber, L. and Gertler, M. Mathematical formulation of bodies of revolution, the David W. *Taylor Model Basin Report*, 719, 1950.

[29] Carichner, G.E. and Nicolai, L.M. *Fundamentals of Aircraft and Airship Design: Volume 2-Airship Design and Case Studies*. American Institute of Aeronautics and Astronautics, 2013.

[30] Meng, J., Li, M., Zhang, L., Lv, M. and Liu, L. Aerodynamic performance analysis of hybrid air vehicles with large reynolds number, In 2019 IEEE *International Conference on Unmanned Systems (ICUS)*, pp 403–409. IEEE, 2019.

[31] Tuveri, M., Ceruti, A. and Marzocca, P. Added masses computation for unconventional airships and aerostats through geometric shape evaluation and meshing, *Int J Aeronaut Space Sci*, 2014, **15**, (3), pp 241–257.

[32] Ceruti, A., Bombardi, T. and Marzocca, P. A CAD environment for the fast computation of added masses. *Ocean Eng*, 2017, **142**, pp 329–337.

[33] Suvarna, S., Chung, H. and Pant, R.S. Optimization of fins to minimize directional instability in airships, *J Aircr*, 2022, **59**(2), pp 317–328.

[34] Sadraey, M.H. *Aircraft Design: A Systems Engineering Approach*. John Wiley & Sons, 2012.

[35] Yanxiang, C., Yanchu, Y., Jianghua, Z., Xiangqiang, Z., et al. Numerical aerodynamic investigations on stratospheric airships of different tail configurations. In 2015 *IEEE Aerospace Conference*, pp 1–9. IEEE, 2015.

[36] Gupta, P., Tripathi, M. and Pant, R.S. Aerodynamic analysis of axi-symmetric lighter-than-air vehicles. In *AIAA Aviation 2021 Forum*, p 2987, 2021.

[37] Kale, S., Joshi, P. and Pant, R. A generic methodology for determination of drag coefficient of an aerostat envelope using CFD, In *AIAA 5th ATIO and16th Lighter-Than-Air Sys Tech. and Balloon Systems Conferences*, p 7442, 2005.

[38] Kungl, P., Schlenker, M. and Kröplin, B. Research and testing activities with the solar powered airship lotte within the scope of the airship research group at the university of Stuttgart, In *14th AIAA Lighter-Than-Air Conference and Exhibition, Akron, Ohio (USA)*, 2001.

Appendix

Standard envelope profiles

The following section introduces some of the standard shapes which have been used for airships for various applications.

A. NPL profile

NPL is a low-drag profile suitable for airship envelopes suggested by National Physics Laboratory [37]. The NPL shape shown in Fig. 33 consists of two ellipsoids of revolution with the major axis of the rear ellipsoid is $\sqrt{2}$ times the major axis of the front ellipsoid. The mathematical representation for a general ellipsoid is:

$$\frac{x^2}{a^2} + \frac{y^2}{b^2} + \frac{z^2}{b^2} = 1 \tag{A1}$$

The 3-D shape of the envelope can also be described by revolving the 2-D shape by 360° about the x-axis. The 2-D shape of the body can be defined by:

$$\frac{x^2}{a^2} + \frac{y^2}{b^2} = 1 \tag{A2}$$

The profile equation of the NPL shape is given by:

$$\begin{cases} y = \pm b\sqrt{1 - (x-a)^2/a^2} & \text{for} \quad x \leq a \\ y = \pm b\sqrt{1 - (x-a)^2/2a^2} & \text{for} \quad x > a \end{cases} \tag{A3}$$

where *a* and *b* are major and minor radii and are design variables of the airship envelope.

B. Zhiyuan-1

The zhiyuan-1 shape shown in Fig. 34 is one of the complex shapes of an airship envelope and consists of various terms and constants.

Table 12. *Zhiyuan-1 profile*

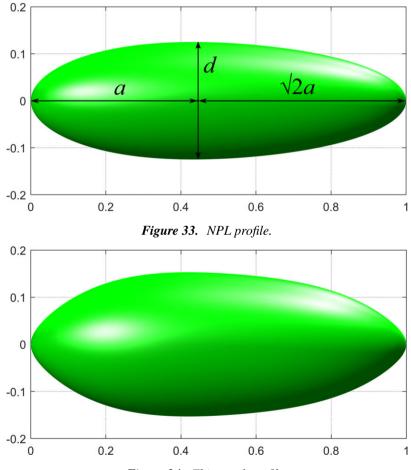| Section	Shape equation
$0 \leq x \leq x_m, z = \dfrac{x}{x_m}$	$y(x) = \dfrac{[r_n F_1(z) + k_1 F_2(z) + G_1(z)]^{1/2}}{2f_r}$
$x_m \leq x < x_p, z = \dfrac{1-x}{1-x_m}$	$y(x) = \dfrac{1}{2f_r} \left[s_t^2 F_3(z) + \left(\dfrac{1-x_m}{x_m} \right)^2 k_1 F_4(z) + G_2(z) \right]^{1/2}$
$x_p \leq x \leq 1.0, z = x$	$y(x) = \dfrac{\left[c_p(1-z) \right]^{1/2}}{2f_r}$

Figure 33. *NPL profile.*

Figure 34. *Zhiyuan-1 profile.*

The details of the functions used in the equations are shown in Table 12:

$$
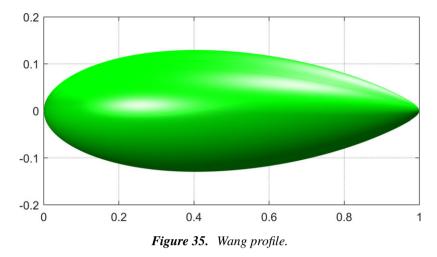\begin{cases}
F_1(z) = -2z(z-1)^3 \\
F_2(z) = -z^2(z-1)^2 \\
G_1(z) = z^2 \left(3z^2 - 8z + 6 \right) \\
F_3(z) = -z^2(z-1)^3 \\
F_4(z) = -z^3(z-1)^2 \\
G_2(z) = z^3 \left(6z^2 - 15z + 10 \right)
\end{cases}
\tag{B1}
$$

Figure 35. *Wang profile.*

The value of constants used in the equations were $r_n = 0.5071$, $k_1 = 0.2913$, $f_r = 3.2992$, $x_p = 0.7570$, $s_t = 3.2361$, $x_m = 0.3936$ and $c_p = 2.7351$.

C. Wang profile

The generatrix of this envelope shown in Fig. 35 is governed by four shape parametres, namely a, b, c, and d and also by the length l. The 3-D geometry of the envelope is expressed as:

$$64 \left(y^2 + z^2\right) = a \left(l - x\right) \left(bx - l\sqrt{c} + \sqrt{cl^2 - dlx}\right) \tag{C1}$$

The 2-D shape equation can be expressed as:

$$y = \frac{\sqrt{a(l - x) \left(bx - l\sqrt{c} + \sqrt{cl^2 - dlx}\right)}}{8} \tag{C2}$$

D. LOTTE profile

LOTTE was the world's first autonomous flying solar-powered airship built by Prof. Bernd Helmut Kröplin and his team in Stuttgart (Germany). Mission areas of this novel solar-powered airship were aerial photography, traffic monitoring, forest fire monitoring, border surveillance and many more. This airship has also been utilised as a reference configuration for theoretical and experimental investigations to evaluate the efficacy of onboard instrumentation, required to carry out successful remote-controlled autonomous flights [38].

The profile of LOTTE shown in Fig. 36 is divided into two sections and is defined by a root function and a polynomial function shown in Equation (D1).

$$\bar{y}(\bar{x}) = \begin{cases} c\sqrt{\bar{x}} & \text{for} \quad 0.0 \leq \bar{x} \leq 0.08 \\ c_0 + c_1\bar{x} + c_2\bar{x}^2 + c_3\bar{x}^3 + c_4\bar{x}^4 + c_5\bar{x}^5 & \text{for} \quad 0.08 \leq \bar{x} \leq 1.0 \end{cases} \tag{D1}$$

where, $\bar{x} = x/L$ and $\bar{y} = y/L$ are the normalised coordinates with respect to the length of the airship (L) in the axial and the radial directions, respectively. Values pertaining to the coefficients of LOTTE polynomial functions are given in Table 13.

E. GNVR profile

The profile of a GNVR-shaped airship comprises three geometrical constructs, namely ellipse, circle and parabola. The profile was named after the late Prof. G.N.V. Rao of IISc, Bengaluru. The entire envelope shape shown in Fig. 37 is parameterised in terms of its maximum diameter (D), as follows:

Table 13. *Coefficients of polynomial function*

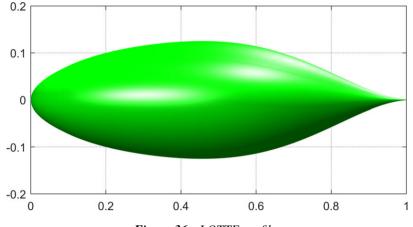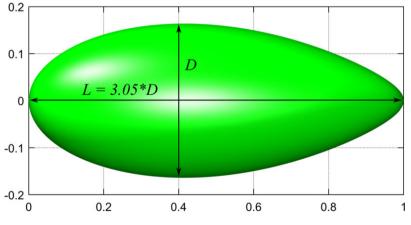| Coefficient	c	c_0	c_1	c_2	c_3	c_4	c_5
Value	0.2277	0.0197	0.7184	−2.3751	5.0166	−5.8339	2.4551

Figure 36. *LOTTE profile.*

Figure 37. *GNVR profile.*

$$y(x) = \begin{pmatrix} 0.5D\sqrt{1 - \left(\dfrac{x - 1.25D}{1.25D}\right)^2} & 0 < x < 1.25D \\ \sqrt{16D^2 - (x - 1.25D)^2} - 3.5D & 1.25D \leq x \leq 2.875D \\ \sqrt{0.1373D\,(1.8D - (x - 1.25D))} & 2.875D \leq x \leq 3.05D \end{pmatrix} \tag{E1}$$

F. Garg profile

Garg et al. [23] considered the hull shape shown in Fig. 38 to optimise the design parameters corresponding to the size and layout of the solar array and to estimate the solar energy required by the airship for the given mission requirements. The envelope profile can be derived from the following expressions:
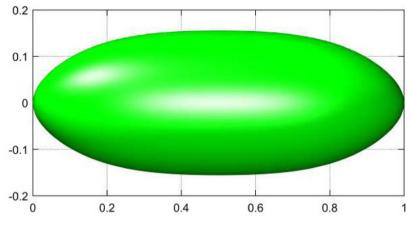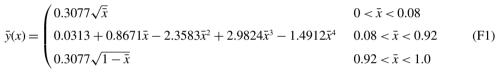
Figure 38. *Garg profile.*

$$\bar{y}(x) = \begin{cases} 0.3077\sqrt{\bar{x}} & 0 < \bar{x} < 0.08 \\ 0.0313 + 0.8671\bar{x} - 2.3583\bar{x}^2 + 2.9824\bar{x}^3 - 1.4912\bar{x}^4 & 0.08 < \bar{x} < 0.92 \\ 0.3077\sqrt{1-\bar{x}} & 0.92 < \bar{x} < 1.0 \end{cases} \qquad \text{(F1)}$$

where $\bar{x} = x/L$ and $\bar{y} = y/L$.